Research Article | Vol. 27, No. 18 / 2 September 2019 / Optics Express 25428
Optics EXPRESS

Conical refraction with low-coherence light sources

V. Yu. Mylnikov,[1] S. N. Losev,[1] V. V. Dudelev,[2] K. A. Fedorova,[3] E. U. Rafailov,[4] and G. S. Sokolovskii[1,5,*]

[1]Ioffe Institute, 26 Polytechnicheskaya str., St. Petersburg, 194021, Russia
[2]ITMO University, 49 Kronverksky pr., St. Petersburg, 197101, Russia
[3]Department of Physics, Philipps-Universität Marburg, Marburg, 35032, Germany
[4]School of Engineering and Applied Science, Aston University, Aston Triangle, Birmingham, B4 7ET, UK
[5]St. Petersburg Electrotechnical University (LETI), St. Petersburg, 197022, Russia
*gs@mail.ioffe.ru

Abstract: We report on conical refraction (CR) with low-coherence light sources, such as light-emitting diodes and decoherentized HeNe laser radiation, and demonstrate different CR patterns. In our experiments, a variation of the pinhole sizes from 25 to 100 μm and the distances to pinhole from 50 to 5 cm reduced spatial coherence of radiation that resulted in the disappearance of the dark Poggendorff's ring in the Lloyd's plane. This is attributed to the interference nature of the Lloyd's distribution and found to be in excellent agreement with the paraxial dual-cone model of conical refraction.

1. Introduction

In 1832, W.R. Hamilton first used the Fresnel wave-surface to calculate the evolution of a narrow non-diverging beam of light propagating along the optical axis of a biaxial crystal [1]. In result of this evolution, a narrow beam will refract as a hollow light cylinder yielding an annular transverse intensity pattern behind the exit facet of the crystal. This research became a starting point for almost two-centuries-long study of the phenomenon of Conical Refraction (CR). The same year, CR was experimentally observed by H. Lloyd [2]. However, Lloyd did not report on a dark ring in the circular intensity pattern of CR that was observed by Poggendorff a few years later in 1839 [3]. More than a century after the discovery of conical refraction, in 1941, Raman published a letter to Nature reporting on the 'focusing' properties of CR pattern [4], the feature nowadays known as Raman spots, which complete the typical evolution of the CR pattern between Lloyd's distribution, Poggendorff's rings and Raman spots as shown in Fig. 1.

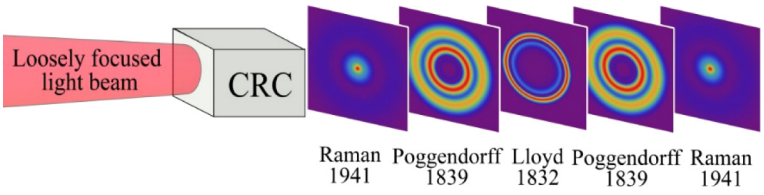

Fig. 1. Evolution of a light beam loosely focused through a conically refracting crystal (CRC).

However, the list of practical applications of CR for many years seemed to be shorter than the list of its features. This was partially associated with the technical difficulties of cutting the biaxial crystals with the necessary precision. Nevertheless, recent publications report on the ultra-efficient CR lasers [5], lasers with CR output [6,7], polarization demultiplexing and multiplexing by means of CR [8], utilization of CR for polarization metrology [9] and for the

#372707 https://doi.org/10.1364/OE.27.025428
Journal © 2019 Received 15 Jul 2019; revised 8 Aug 2019; accepted 8 Aug 2019; published 22 Aug 2019

Optics EXPRESS

generation and annihilation of optical vortices [10]. A considerable amount of other practical applications was thoroughly reviewed in [11]. Undoubtedly, advanced applications of CR were enabled by the progress in theoretical description of the CR phenomenon.

Interestingly, the dark Poggendorff's ring remained unexplained for a long time after its discovery until the Voigt's publication in 1905 [12]. His interpretation relays on proportionality of the divergence of the conical refraction pattern inside a biaxial crystal to the divergence of an initial beam propagating along the optical axis. From this fact, zero light intensity at zero divergence angle is derived using the proportionality of the total beam energy to the beam divergence angle. This explanation is widely accepted nowadays and cited in textbooks on optics [13] despite the fact that similar interpretation may result in a dark region inside any (not only conically) refracted pattern. To the contrary, the interpretation of Raman spots as a 'self-focusing' feature of CR given at the time of its observation is still valid. Nevertheless, important features such as concentric fringes around Raman spots and oscillations decorating the inner ring of the Lloyd's double-ring (that can be regarded as a 'prelude' to the Raman spot) were explained only recently by M. Berry in his seminal work [14] as a product of self-interference (or 'diffraction') of the inner Lloyd's ring. However, the interference was not considered to be the origin of the dark Poggendorff's ring in the abovementioned publications. In this work, we present the results of experiments on conical refraction with narrow-apertured low-coherence light sources, such as light-emitting diodes (LEDs) and a HeNe laser, and demonstrate that an increase of the pinhole size or reduction of the distance to pinhole results in the disappearance of the dark ring separating the Lloyd's counterparts. We attribute this to the interference nature of the Lloyd's distribution and explain the experimental data within the paraxial dual-cone model of conical refraction [15,16].

2. Theory

For theoretical description of the CR phenomenon we use the general solution derived by A.M. Belsky and A.P. Khapalyuk [17] and by M.V. Berry [18]. According to these, for unpolarised light passing through the CR crystal we can write the light intensity in the form [18]:

$$I = |B_0|^2 + |B_1|^2. \tag{1}$$

With the functions B_m defined as:

$$B_m = k\int_0^\infty Pa(P)e^{-ikZP^2/2}\cos(kR_0P - m\frac{\pi}{2})J_m(kRP)dP. \tag{2}$$

where $m = 0,1$ is the integer number, k is the light wavevector, kP is the transverse wavevector (with $P<<1$ because of paraxiality), R_0 is the radius of conical refraction beyond the crystal, Z is the normalized distance, J_m is the Bessel function of the first kind of order m, and $a(P)$ is the Fourier transform of the incident beam.

From (1) one can immediately see that due to the absence of interference between B_0 and B_1 [18], it is impossible to introduce directly the coherence of the incident beam. Therefore, we utilize the recently proposed paraxial dual-cone model of CR that takes into account the effect of interference [15–16]. According to this model, vector of electric field can be described as a superposition of two conically-propagating vector components $\vec{C}_1$ and $\vec{C}_{-1}$, correspondingly:

$$\vec{C}_q = \sum_{s=\pm1}\vec{e}_s(\varphi)(\vec{e}_s(\varphi)\cdot\vec{e}_{in})\left[\frac{k}{2}\int_0^\infty Pa(P)e^{-ikZP^2/2+iqkR_0P}\{J_0(kRP) - iqsJ_1(kRP)\}dP\right]. \tag{3}$$

$$\vec{e}_1(\varphi) = (cos(\varphi/2),\ sin(\varphi/2)),\quad \vec{e}_{-1}(\varphi) = (sin(\varphi/2), -cos(\varphi/2)). \tag{4}$$

where q and s are the indices that take values of 1 and -1, $\vec{e}_{in}$ is the vector of polarization of the input beam, and φ is the azimuthal angle. In this form $\vec{C}_1$ and $\vec{C}_{-1}$ are two cones that converge

Optics EXPRESS

and diverge behind the exit plane of the conically-refracting crystal and intersect in the Lloyd's plane. The light intensity is then given by:

$$I = |\vec{C}_1 + \vec{C}_{-1}|^2 \tag{5}$$

Formula (5) clearly shows the critical importance of the interference between $\vec{C}_1$ and $\vec{C}_{-1}$ for the correct representation of a CR pattern. For the partially coherent light we can introduce the coherence degree α [13] and describe the intensity distribution in the Lloyd's plane as the interference of the cones in the form:

$$I = |\vec{C}_1|^2 + |\vec{C}_{-1}|^2 + \alpha(\vec{C}_1 \cdot \vec{C}^*_{-1} + \vec{C}_1 \cdot \vec{C}^*_{-1}). \tag{6}$$

When $\alpha \rightarrow 1$ the light is completely coherent and the interference term is important in (6) so that:

$$I_{\alpha \rightarrow 1} \approx |\vec{C}_1|^2 + |\vec{C}_{-1}|^2 + \vec{C}_1 \cdot \vec{C}^*_{-1} + \vec{C}_1 \cdot \vec{C}^*_{-1}. \tag{7}$$

With $\alpha << 1$ the light is incoherent and the interference contribution in (6) tends to zero and this leads to the total disappearance of the interference between two cones in the plane of intersection, i.e. in the Lloyd's plane.

$$I = |\vec{C}_1|^2 + |\vec{C}_{-1}|^2. \tag{8}$$

Equations (7) and (8) represent the CR patterns for the coherent and incoherent radiation, correspondingly. Using the Van Cittert–Zernike theorem, the spatial coherence degree of partially coherent light from an absolutely incoherent source can be written in the form [19]:

$$\alpha = \left| \frac{2J_1(x)}{x} \right|; x = kD\frac{r_s}{L_1} \tag{9}$$

where r_s is the source radius, D is the pinhole diameter and L_1 is the distance between the source and pinhole. From (9) it is easy to see that α increases with the decrease of the pinhole diameter D and as the distance L_1 from the source to the pinhole increases.

The effect of the interference between the intersecting cones $\vec{C}_1$ and $\vec{C}_{-1}$ in the Lloyd's plane is shown in Fig. 2. One can see the clear Poggendorff's dark ring in Fig. 2(a) where the Lloyd's

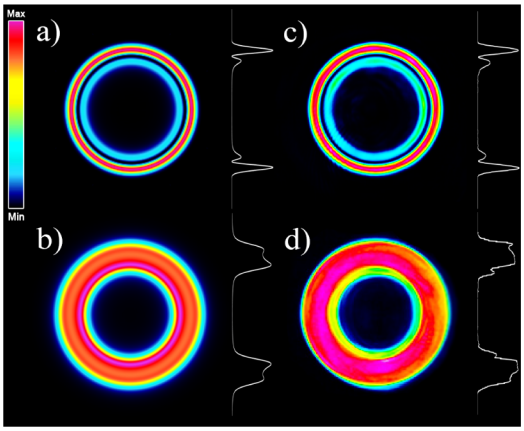

Fig. 2. Lloyd's distribution of the CR beam intensity computed numerically from the dual-cone model with the Gaussian beam and coherence degree α=1 (a) or the flattened Gaussian beam and α=0 (b). Conical refraction pattern in the Lloyd`s plane for coherent (c) and decoherentized laser beam (d). Laser beam is decoherentized by the rotating blurry plate. Beam intensity profiles are shown on the right of each pattern.

Optics EXPRESS

distribution is simulated with Eq. (7) for a Gaussian input beam. In Fig. 2(b), a similar simulation was performed with Eq. (8) for the flattened Gaussian beam with 'flattening' parameter N = 3 [20] that results in a single light ring in the Lloyd's plane and the absolute absence of the dark one. Numerical simulations of the axial distribution of a CR pattern with a coherent (α=1) and an incoherent (α=0) beam is shown in Figs. 4(a) and 4(c) and Fig. 4(b), correspondingly. One can see the clear interference pattern in Figs. 4(a) and 4(c) and intersection of two light cones without any sign of interference in Fig. 4(b). The difference between the Lloyd's patterns in Figs. 4(a) and 4(c) should also be noted. The reason for that is the difference in the spatial distribution of the illuminating light source being the coherent Gaussian beam for Fig. 4(a) and coherently illuminated pinhole for Fig. 4(c) [18].

3. Experiment

In our experiments, we used two types of light sources: a HeNe laser and a LED. Using the HeNe laser ($\lambda \approx 632.8$ nm), the typical conical refraction pattern with clearly defined double ring distribution in the Lloyd's plane can be easily observed, as seen in Fig. 2(c). To reduce spatial coherence of the laser beam we used a rotating blurry plate and a 100 μm pinhole. This leads to the total disappearance of the dark ring in the Lloyd's plane, as shown in Fig. 2(d). We also used a high-power red LED with the central wavelength $\lambda \approx 619$ nm as a light source. The spectrum of LED radiation is shown in Fig. 3(a). From this spectrum, it is easy to see that the full width at half-maximum (FWHM) of the LED emission was about 15 nm.

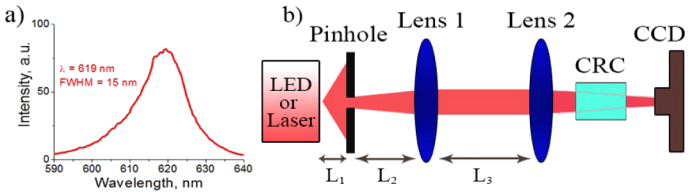

Fig. 3. (a) LED emission spectrum; (b) Schematic of the optical setup used for the CR experiments with low-coherence light sources. Pinholed LED radiation was collimated by a Lens 1 (of variable focal length) and then focused by a Lens 2 (focal length 100 mm) through a CRC. The CCD camera detecting an output pattern was mounted on a long-range translation stage enabling registration of the spatial evolution of the conically refracted LED radiation.

With such a wide spectrum of radiation, the temporal coherence length can be estimated to be as short as ~26 μm. However, even such a small value appears to be long enough for observation of the interference effects in our experiments. Because of paraxiality, the minimum required temporal coherence length is as short as ~1 μm. Therefore, special care must be taken on the spatial coherence of the LED radiation via the utilization of pin-holes of different diameters and by variation of the distance from the light source to the pinhole. The diffractive divergence of the LED light after a pinhole was compensated with a collimating lens. A similar technique was used in the first CR experiments performed long before the introduction of lasers. Also, a collimating lens can be replaced with an iris aperture as demonstrated in a recent publication on white-LED-light CR [21].

The schematic setup used in our experiments is shown in Fig. 3(b). The light radiation was transmitted through a pinhole of either 25 or 100 μm in diameter and collimated with the Lens 1 of variable focal length. The degree of coherence of the collimated narrow-apertured radiation was approximated to be close to unity. On the other hand, the coherence of the widely-apertured light radiation was tending to zero with the short distance (5 cm) to the pinhole and close to unity with the long distance of 50 cm. The collimated light was focused with the Lens 2 of 100 mm

Optics EXPRESS

focal length into a 18-mm long KGW crystal cut along the optical axis. The output pattern of the CR was detected with a CCD camera mounted on a high-precision translation stage with travel range of 150 mm.

With high spatial coherence of LED light achieved via the utilization of the narrow 25 μm pinhole one can observe the classical CR pattern with a clearly defined dark ring in the Lloyd's plane as shown in Fig. 4(d). With an increase of a pinhole size to 100 μm and reduction of the distance to pinhole L_1 to 5 cm, the spatial coherence of LED light tends to zero. This leads to the same pattern (Fig. 4(e)) as for the laser beam radiation after the blurry rotating plate, that was mentioned earlier. Having this in mind, we assume that the dark ring was not observed by H. Lloyd in the first experiment on conical refraction [2] only because of the insufficient spatial coherence of light preventing the interference of the diverging and converging cones in the CR pattern. The spatial coherence can be further improved by increasing the distance from the LED to the pinhole. The axial distribution of the experimental CR pattern for the 100 μm pinhole and L_1=50 cm is shown in Fig. 4(f). These experimental results are in very good agreement with numerical simulations according to (7) and (8), as shown in Figs. 4(a)–4(c). We also note the observation of axial oscillations of the Raman spot intensity in Figs. 4(c) and 4(f). However, we leave the detailed research on this matter for the future work.

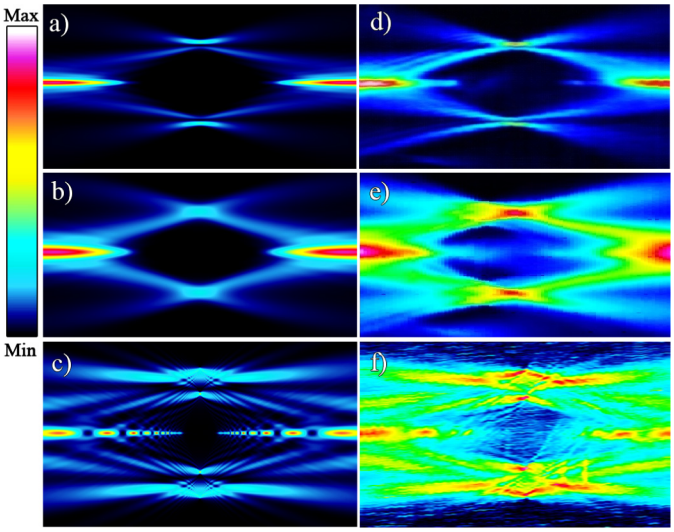

Fig. 4. The axial distribution of the CR beam intensity computed numerically from the dual-cone model with the Gaussian beam and coherence degree α=1 (a) or α=0 (b) and coherently illuminated pinhole (c). Conical refraction pattern with LED light along the beam propagation axis with a pinhole size and distance to pinhole of 25 μm and 5 cm (d), 100 μm and 5 cm (e), 100 μm and 50 cm (f), correspondingly. Note the difference in the horizontal and vertical scales: the distance between Raman spots (horizontal) is ~50 mm, the diameter of the Lloyd ring (vertical) is ~0.6 mm.

Figure 5 presents the transition from spatially coherent CR (first column) to incoherent CR (fourth column) with a partially coherent light in the middle (second and third column). First row shows experimental transverse distributions while the second one presents the results of corresponding numerical simulations according to (6) and (9) for a flattened Gaussian beam with 'flattening' parameter N = 3 [20]. Visualization 1 shows experimental transformation of the Lloyd's pattern with the spatial coherence degree α varying from 0.07 to 0.85.

Finally, using collimating lenses with different focal length (Lens 1 in Fig. 3) we were able to change the fundamental parameter $\rho_0 = R_0/w_0$ of the conical refraction in our experiments.

Optics EXPRESS

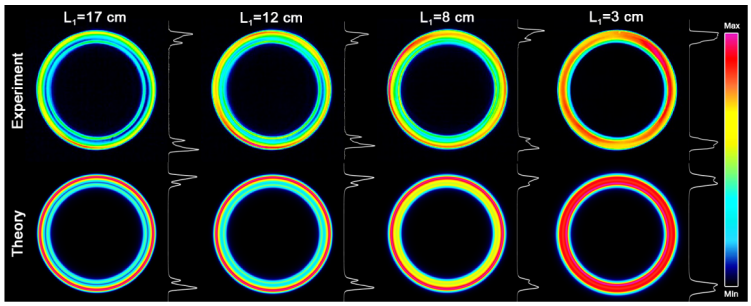

Fig. 5. Transverse intensity distributions of the CR beam at Z = 0 (Lloyd's plane) obtained experimentally (first row) and from numerical simulations (second row) for a 100 μm pinhole diameter and a distance from the LED to pinhole $L_1 \sim 17$ cm (α=0.85, first column), 12 cm (α=0.74, second column), 8 cm (α=0.54, third column) and 3 cm (α=0.07, fourth column), correspondingly. Beam intensity profiles are shown on the right of each pattern. Visualization 1 shows experimental transformation of the Lloyd's distribution with α varying from 0.07 to 0.95.

Figure 6(a) compares transverse CR intensity patterns for unpolarized LED radiation produced by coherent and incoherent light for ρ_0 = 1.2, 1.7, 2.7, 4.5 and 10. Figure 6(b) shows the Lloyd's distributions for the linearly polarized light for the same values of ρ_0 as Fig. 6(a). It can be

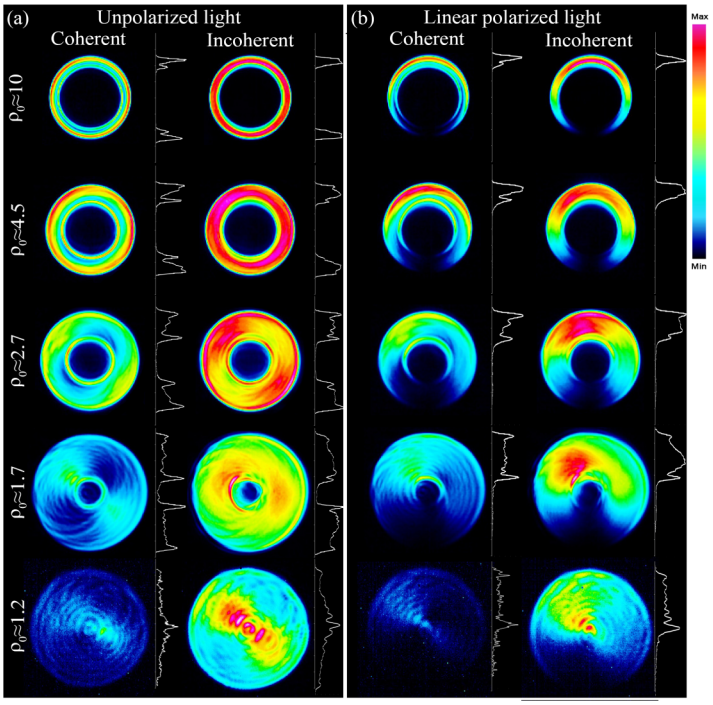

Fig. 6. Measured Lloyd's pattern for unpolarized LED radiation (a) and linear polarized light (b). Parameter $\rho_0 = R_0/w_0 \approx 10$ (first row), $\rho_0 \approx 4.5$ (second row), $\rho_0 \approx 2.7$ (third row), $\rho_0 \approx 1.7$ (fourth row) and $\rho_0 \approx 1.2$ (fifth row). For each box, the first column corresponds to coherent light ($\alpha \approx 1$), while the second column to incoherent ($\alpha \approx 0$). Beam intensity profiles are shown on the right of each pattern.

Optics EXPRESS

clearly seen that for the linear polarized incoherent LED radiation a crescent-shaped distribution is still observed, as for the coherent light.

4. Conclusion

In conclusion, we performed the experiments on conical refraction with low-coherence light sources. To do this, we utilized LED radiation pinholed to 25 or 100 μm in a distance of 50 mm or 500 mm and HeNe laser light decoherentized with a rotating blurry plate. The narrow-apertured radiation produced the classical CR pattern with a clearly defined dark Poggendorff's ring in the Lloyd's plane. Similarly, the wider-apertured radiation with a longer distance from the light source to the pinhole also produced a well-defined dark ring in the Lloyd's plane. On the opposite, the incoherent wider-apertured radiation with a short distance to the pinhole produced the Lloyd's distribution comprising a single light ring without any sign of the dark counterpart. These results are naturally explained within the paraxial dual-cone model of CR [15–16], where the CR pattern in the Lloyd's plane is described in terms of the interference between the cones diverging and converging behind the CR crystal. Therefore, the utilization of incoherent light in the CR experiment eliminates the interference of the cones and removes the fine dual-ring structure from the Lloyd's pattern. These results may significantly affect the existing practical applications of CR, including optical trapping with CR beams [22] and formation of robust optical bottles [23] in which particles may be trapped by means of, for example, the photophoretic effect. Here, one should also name the utilization of CR for quantum computing and cryptography [24], and super-resolution microscopy [25]. CR with incoherent light may boost the new applications such as very cost-efficient generation of bottle-beams and annular field patterns for object tracking and localization [26], generation of polarization vortices [27], producing novel optical fields, such as Janus waves [28] and many other applications in imaging and lithography.

References

1. W. R. Hamilton, "Third supplement to an essay on the theory of systems of rays," Trans. R. Irish Acad. **17**, 1–144 (1833).
2. H. Lloyd, "On the phenomena presented by light in its passage along the axes of biaxial crystals," Philos. Mag. **1**(1), 112–114 (1833).
3. J. C. Poggendorff, "Ueber die konische Refraction," Ann. Phys. (Berlin, Ger.) **124**(11), 461–462 (1839).
4. C. V. Raman, V. S. Rajagopalan, and T. M. K. Nedungadi, "The phenomena of conical refraction," Nature **147**(3722), 268 (1941).
5. A. Abdolvand, K. G. Wilcox, T. K. Kalkandjiev, and E. U. Rafailov, "Conical refraction Nd:$KGd(WO_4)_2$ laser," Opt. Express **18**(3), 2753–2759 (2010).
6. Yu. V. Loiko, G. S. Sokolovskii, D. J. Carnegie, A. Turpin, J. Mompart, and E. U. Rafailov, "*Laser beams with conical refraction patterns*," *Proc. SPIE 8960*, 89601Q (2014).
7. R. Akbari, C. Howlader, K. A. Fedorova, G. S. Sokolovskii, E. U. Rafailov, and A. Major, "Conical refraction output from a Nd:YVO_4 laser with an intracavity conerefringent element," Opt. Lett. **44**(3), 642–645 (2019).
8. A. Turpin, Yu. V. Loiko, T. K. Kalkandjiev, and J. Mompart, "Free-space optical polarization demultiplexing and multiplexing by means of conical refraction," Opt. Lett. **37**(20), 4197–4199 (2012).
9. A. Peinado, A. Turpin, A. Lizana, E. Fernandez, J. Mompart, and J. Campos, "Conical refraction as a tool for polarization metrology," Opt. Lett. **38**(20), 4100–4103 (2013).
10. D. P. O'Dwyer, C. F. Phelan, Y. P. Rakovich, P. R. Eastham, J. G. Lunney, and J. F. Donegan, "The creation and annihilation of optical vortices using cascade conical diffraction," Opt. Express **19**(3), 2580–2588 (2011).
11. A. Turpin, Y. V. Loiko, T. K. Kalkandjiev, and J. Mompart, "Conical refraction: Fundamentals and applications," Laser Photonics Rev. **10**(5), 750–771 (2016).
12. W. Voigt, "Bemerkung zur theorie der konischen refraction," Phys. Z. **6**, 672–673 (1905).
13. M. Born and E. Wolf, *Principles of Optics* (Cambridge University, 1999).
14. M. V. Berry, M. R. Jeffrey, and J. G. Lunney, "Conical diffraction: observations and theory," Proc. R. Soc. A **462**(2070), 1629–1642 (2006).
15. G. S. Sokolovskii, D. J. Carnegie, T. K. Kalkandjiev, and E. U. Rafailov, "Conical Refraction: New observations and a dual cone model," Opt. Express **21**(9), 11125–11131 (2013).
16. A. Turpin, Yu. Loiko, T. K. Kalkandjiev, H. Tomizawa, and J. Mompart Turpin, "On the dual-cone nature of the conical refraction phenomenon," Opt. Lett. **40**(8), 1639–1642 (2015).

Optics EXPRESS

17. A. M. Belskii and A. P. Khapaluyk, "Internal conical refraction of bounded light beams in biaxial crystals," Opt. Spectrosc. **44**(4), 436–439 (1978).
18. M. V. Berry, "Conical diffraction asymptotics: fine structure of Poggendorff rings and axial spike," J. Opt. A: Pure Appl. Opt. **6**(4), 289–300 (2004).
19. L. Mandel and E. Wolf, *Optical Coherence and Quantum Optics* (Cambridge University, 1995).
20. F. Saad and A. Belafhal, "A detailed study of internal conical refraction phenomenon of flattened Gaussian beams propagating in a biaxial crystal," Optik **138**, 145–152 (2017).
21. R. T. Darcy, D. McCloskey, K. E. Ballantine, B. D. Jennings, J. G. Lunney, P. R. Eastham, and J. F. Donegan, "White light conical diffraction," Opt. Express **21**(17), 20394–20403 (2013).
22. C. McDougall, R. Henderson, D. J. Carnegie, G. S. Sokolovskii, E. U. Rafailov, and D. McGloin, "*Flexible particle manipulation techniques with conical refraction-based optical tweezers*," *Proc. SPIE 8458*, 845824 (2012).
23. A. Turpin, V. Shvedov, C. Hnatovsky, Yu. V. Loiko, J. Mompart, and W. Krolikowski, "Optical vault: A reconfigurable bottle beam based on conical refraction of light," Opt. Express **21**(22), 26335–26340 (2013).
24. D. P. O'Dwyer, C. F. Phelan, Y. P. Rakovich, P. R. Eastham, J. G. Lunney, and J. F. Donegan, "Generation of continuously tunable fractional optical orbital angular momentum using internal conical diffraction," Opt. Express **18**(16), 16480–16485 (2010).
25. S. Rosen, G. Y. Sirat, H. Ilan, and A. J. Agranat, "A sub wavelength localization scheme in optical imaging using conical diffraction," Opt. Express **21**(8), 10133–10138 (2013).
26. G. Xie, L. Li, Y. Ren, Y. Yan, N. Ahmed, Z. Zhao, C. Bao, Z. Wang, C. Liu, H. Song, R. Zhang, K. Pang, S. Ashrafi, M. Tur, and A. E. Willner, "Localization from the unique intensity gradient of an orbital-angular-momentum beam," Opt. Lett. **42**(3), 395–398 (2017).
27. S. Fu, C. Gao, Y. Shi, K. Dai, L. Zhong, and S. Zhang, "Generating polarization vortices by using helical beams and a Twyman Green interferometer," Opt. Lett. **40**(8), 1775–1778 (2015).
28. D. G. Papazoglou, V. Yu. Fedorov, and S. Tzortzakis, "Janus waves," Opt. Lett. **41**(20), 4656–4659 (2016).